

January 15, 2013

Massive Galaxies at High- z : Assembly Patterns, Structure & Dynamics in the Fast Phase of Galaxy Formation

J. Oñorbe^{1,2}, F.J. Martínez-Serrano³, R. Domínguez-Tenreiro¹, A. Knebe¹ and A. Serna³

jonorbeb@uci.edu

ABSTRACT

Relaxed, massive galactic objects have been identified at redshifts $z = 4, 5$, and 6 in hydrodynamical simulations run in a large cosmological volume. This allowed us to analyze the assembly patterns of the high mass end of the galaxy distribution at these high z s, by focusing on their structural and dynamical properties. Our simulations indicate that massive objects at high redshift already follow certain scaling relations. These relations define virial planes at the halo scale, whereas at the galactic scale they define *intrinsic dynamical planes* that are, however, tilted relative to the virial plane. Therefore, we predict that massive galaxies must lie on fundamental planes from their formation.

We briefly discuss the physical origin of the tilt in terms the physical processes underlying massive galaxy formation at high z , in the context of a two-phase galaxy formation scenario. Specifically, we have found that it lies on the different behavior of the gravitationally heated gas as compared with cold gas previously involved in caustic formation, and the mass dependence of the energy available to heat the gas.

Subject headings: galaxies: elliptical and lenticular, cD — galaxies: Evolution — galaxies: Formation — galaxies: Fundamental Parameters — hydrodynamics — methods: numerical

¹Grupo de Astrofísica, Departamento de Física Teórica, Modulo C-15, Universidad Autónoma de Madrid, Cantoblanco E-28049, Spain

²Department of Physics and Astronomy, University of California at Irvine, Irvine, CA 92697, USA

³Depto. de Física y A.C., Universidad Miguel Hernández, E-03202 Elche, Alicante, Spain

1. Introduction

One of the outstanding yet most important problems in astrophysics is how and when galaxies formed within the framework of the expanding Universe described by the concordance model of cosmology. Massive galaxies at high z become more and more important to study. In fact, the availability of multi-wavelength data from new generations of deep surveys, including wide field panoramic surveys, allowed for searches for such massive galaxy candidates up to $z \simeq 4 - 6.5$ (Giavalisco et al. 2004; Mobasher et al. 2005; McLure et al. 2006; Yan et al. 2006; Rodighiero et al. 2007; Bouwens et al. 2007; Wiklind et al. 2008; Mancini et al. 2009; Stark et al. 2009; Mobasher & Wiklind 2010; Dahlen et al. 2010; Capak et al. 2011) or even $z \approx 10$ (Bouwens et al. 2011). However, still very few is known about the physical processes underlying the (putative) presence of such massive systems at these high redshifts. In fact, the mere existence of them could seem paradoxical within a direct interpretation of the hierarchical structure formation scenario (e.g. Toomre 1977; White & Rees 1978). Further, such possible contradictions are not necessarily alleviated by the competing monolithic collapse scenario (Eggen, Lynden-Bell & Sandage 1962; Larson 1974) and hence the question about the existence (and the properties) of massive galaxies at high-redshift remains open.

Recently, a scenario has emerged to explain massive galaxy formation that shares characteristics of both the aforementioned classical scenarios, but is nevertheless different. Indeed, analytical models (Salvador-Solé et al. 2005), as well as N-body simulations (Wechsler et al. 2002; Zhao et al. 2003), have shown that two different phases can be distinguished along *halo* mass assembly: i) first, a violent, fast phase, with high mass aggregation (i.e., merger) rates, ii) later on, a slow phase, where the mass aggregation rates are much lower. Hydrodynamical simulations have confirmed this scenario and its implications for properties of massive galactic objects at low z , see Domínguez-Tenreiro et al. (2006), see also Oser et al. (2010) and Cook, Lapi & Granato (2009). Concerning high z s, it has been shown that the fast phase has the characteristics of a *multiclump collapse*, where mergers involve very low relative angular momentum, and, in fact, they are induced by the collapse of flow convergence regions displaying a web-like morphology (Domínguez-Tenreiro et al. 2010).

In this *Letter* we investigate the high mass end of galactic stellar objects at high-redshift ($z = 4, 5$ and 6) obtained by means of self-consistent cosmological simulations within a volume large enough to account for the proper treatment of the large-scale structure yet simultaneously capturing all the relevant small-scale (baryonic) physics. Not only do we investigate their mere presence, we also study whether they had enough time to dynamically relax at such high redshifts. To this end, we have focused on the intrinsic mass (as opposed to luminosity) as well as structural and kinematical properties of these objects at their halo (i.e. virial radius) and stellar/galactic scale (to be defined below) as fingerprints of the

physical processes involved in their assembly.¹ Specifically, we investigate the appearance of samples of high- z massive galactic objects with dynamical planes tilted relative to the virial plane, and link their underlying formation physics to the Adhesion Model (Gurbatov et al. 1989; Vergassola et al. 1994).

Our results here are an extension to higher z s of previous studies on the fundamental plane (FP) at $z = 0$ (Oñorbe et al. 2005, 2006). In these two papers the different possibilities causing the tilt of the FP relative to the virial plane are analyzed in detail. It is shown that if both the virial mass to luminosity ratio, M_{vir}/L , and the mass structure coefficient $c_{\text{M}}^{\text{vir}}$ (see Eqs. 2 and 4 in Oñorbe et al. (2005)) are independent of mass, then no FP tilt would be measured. Here, because mass is considered instead of luminosity and no projection effects are taken into account, we have instead analyzed the mass dependence of the ratio $M_{\text{bo}}^{\text{star}}/M_{\text{vir}}$ and the mass structure coefficient $c_{\text{M}}^{\text{vir}} = (GM_{\text{vir}})/([\sigma_{\text{bo}}^{\text{star}}]^2 r_{\text{e,bo}}^{\text{star}})$, where $M_{\text{bo}}^{\text{star}}$ and $\sigma_{\text{bo}}^{\text{star}}$ are the stellar mass and the 3D stellar velocity dispersion at the galactic scale, respectively, and $r_{\text{e,bo}}^{\text{star}}$ is the 3D stellar mass effective radius also defined at the galactic scale². We need to stress that a mass dependence of either of these quantities automatically implies a tilt of the dynamical plane relative to the virial plane.

2. Structural and kinematical Properties of massive Objects at high- z

The simulations used here are part of the GALFOBS project. They are N -body + SPH simulations that have been performed using an OpenMP parallel version of the DEVA code (Serna, Domínguez-Tenreiro, & Sáiz 2003) and the methods for star formation and cooling described in Martínez-Serrano et al. (2008). The DEVA code pays particular attention to ensure that conservation laws (e.g. momentum, energy, angular momentum, and entropy) hold as accurately as possible³. Star formation is implemented through a Kennicutt-Schmidt-like law with a density threshold ρ_{thres} and a star formation efficiency of c . The values of these parameters implicitly account for star formation regulation by discrete energy injection processes.

¹ We stick to 3D properties as well as mass (instead of luminosity) for two reasons: i) projection effects add noise in the statistical analysis (Oñorbe et al. 2006) and ii) we are not aiming at providing observables but rather at understanding the physical processes involved in the formation of these objects.

²Please refer to Table 1 of Oñorbe et al. (2006) where our nomenclature and definitions are more thoroughly introduced.

³This in particular implies that a double loop in the neighbour searching algorithm must be used, which considerably increases the CPU time.

The main simulation was carried out in a periodic cube of 80 Mpc side length using 512^3 baryonic and 512^3 dark matter particles with a gravitational softening of $\epsilon_g = 2.3$ kpc and a minimum hydrodynamical smoothing length half this value. The cosmology applied was a Λ CDM model whose parameters as well as those of the field of primordial density fluctuations (i.e., initial spectrum) have been taken from CMB anisotropy data⁴ (Dunkley et al. 2009), with $\Omega_m = 0.295$, $\Omega_b = 0.0476$, $\Omega_\Lambda = 0.705$, $h = 0.694$, an initial power-law index $n = 1$, and $\sigma_8 = 0.852$. The mass resolution is $m_{bar} = 2.42 \times 10^7 M_\odot$ and $m_{dm} = 1.26 \times 10^8 M_\odot$ and the star formation parameters used were $\rho_{thres} = 4.79 \times 10^{-25} g cm^{-3}$ and $c = 0.3$.

When analyzing galaxy formation in numerical simulations it is desirable to verify that the objects in the simulation are consistent with observations at low z 's. Due to the extreme CPU consumption by hydrodynamical forces, this is not yet possible for the main GALFOBS simulation. As a way out, we ran three sub-volumes of the main cube using a “zoom approach”. In this approach the gravitational forces have been calculated for the full box whereas the hydrodynamical forces (which are exclusively local) were only computed in a sub-box of side length 26 Mpc. These three sub-volumes have been analysed at redshift $z = 0$ showing that we indeed obtain galaxy populations in agreement with low-redshift observations, as we had also previously shown in Sáiz et al. (2004) using the same approach yet smaller simulation boxes.

Halos in our simulations are identified by the OpenMP+MPI halo finder **AHF**⁵ (Knollmann & Knebe 2009) as well as **SKID** (Weinberg et al. 1997), and their respective results have been cross-compared to check for completeness. The halo scale of these objects is defined by the virial radius (r_{vir}) based upon the Bryan & Norman (1998) fitting function to determine the overdensity threshold. The so-called galactic scale has been based upon material (stars) inside a sphere of radius $r = 0.15 \times r_{vir}$, a scale separating the baryon from the dark matter domination (Bailin et al. 2005). This automated procedure has been tested by comparing with individually determined limiting stellar sizes of several hundred of objects based upon their 3D visualization as well as their 3D stellar density profiles. We further asked that our objects are not involved in violent events, either at the halo or at the galactic scale. To exclude this kind of objects at the halo scale, we have used the form factor, c_F , defined via the virial relation $c_F = (GM_{vir})/([\sigma_h^{tot}]^2 r_{e,h}^{tot})$, where σ_h^{tot} is the velocity dispersion and $r_{e,h}^{tot}$ the half-mass radius at the halo scale, and we asked it to be within the expected interval (1.9, 2.5) for virialized objects (Binney & Tremaine 2008) and of the order of unity if we

⁴ http://lambda.gsfc.nasa.gov/product/map/current/params/lcdm.sz_lens_run_wmap_5_bao_small_lyapost.cfm

⁵ **AHF** can be freely downloaded from <http://popia.ft.uam.es/AMIGA>

use r_{vir} instead of $r_{\text{e,h}}^{\text{tot}}$. The same procedure has been employed on the galactic object scale using – in analogy – the parameter $c_{\text{F}}^{\text{star}} = (GM_{\text{bo}}^{\text{star}})/([\sigma_{\text{bo}}^{\text{star}}]^2 r_{\text{e,bo}}^{\text{star}})$. Again, objects outside a certain range (based upon a manually gauged subsample of 200 objects for each z) have been discarded. Putting a mass threshold of $M_{\text{bo}}^{\text{star}} > 10^{10} M_{\odot}$, our final samples consists of 137, 521 and 1315 galaxies at $z = 6$, $z = 5$ and $z = 4$, respectively, not involved in violent events at any scale.

Our first result is in fact the mere existence of these samples of high-redshift relaxed massive galaxies. To understand their origin, we first quantify the correlation and inter-relation, respectively, between their mass (M_{vir} and $M_{\text{bo}}^{\text{star}}$), size (half-mass radii $r_{\text{e,h}}^{\text{tot}}$ and $r_{\text{e,bo}}^{\text{star}}$) and velocity dispersion⁶ ($\sigma_{\text{h}}^{\text{tot}}$ and $\sigma_{\text{bo}}^{\text{star}}$) both at the halo and at the stellar scale using the following variables: $E_{\text{halo}} \equiv \log_{10} M_{\text{vir}}$, $r_{\text{halo}} \equiv \log_{10} r_{\text{e,h}}^{\text{tot}}$, $v_{\text{halo}} \equiv \log_{10} \sigma_{\text{h}}^{\text{tot}}$, and $E_{\text{star}} \equiv \log_{10} M_{\text{bo}}^{\text{star}}$, $r_{\text{star}} \equiv \log_{10} r_{\text{e,bo}}^{\text{star}}$, $v_{\text{star}} \equiv \log_{10} \sigma_{\text{bo}}^{\text{star}}$. We list the average values \bar{E} , \bar{r} , and \bar{v} in Table 1 where we can observe a mild increase of r_{halo} alongside a decrease of v_{halo} while E_{halo} remains constant: as the Universe expands, the objects become on average less and less compact due to the decrease of the global density (Padmanabhan 1993). We basically observe the same phenomenon on the stellar scale, however, accompanied by a moderate increase in E_{star} . In fact, the ratios $r_{\text{e,h}}^{\text{tot}}/r_{\text{e,bo}}^{\text{star}}$ and $\sigma_{\text{h}}^{\text{tot}}/\sigma_{\text{bo}}^{\text{star}}$ show an scaling behaviour as a function of either M_{vir} or $M_{\text{bo}}^{\text{star}}$ (see Table 2 and below).

Going one step further, we search for planes in the (E, r, v) space by performing a principal component analysis (PCA) of all samples. It is made in 3D to circumvent projection effects (Oñorbe et al. 2006). We have found that at all redshifts one of the eigenvalues of the PCA is considerably smaller than the others, so that (massive) objects populate a flattened ellipsoid close to two-dimensional, both at the halo scale and at the stellar object scale:

$$E_s - \bar{E}_s = \alpha_s^{3\text{D}}(r_s - \bar{r}_s) + \gamma_s^{3\text{D}}(v_s - \bar{v}_s), \quad (1)$$

where s refers to the scale of the object, i.e. halo or star. Table 1 also lists the values of the parameters $\alpha_s^{3\text{D}}$ and $\gamma_s^{3\text{D}}$ of these planes as well as their bootstrapping errors. We find that at the halo scale the planes are close to the virial plane (VP, defined by $(\sigma_{\text{h}}^{\text{tot}})^2 = GM_{\text{vir}}/r_{\text{e,h}}^{\text{tot}}$ or $\alpha_{\text{halo}}^{3\text{D}} = 1, \gamma_{\text{halo}}^{3\text{D}} = 2$), as expected for well-defined haloes. At the stellar scale we also find planes to which we refer as the *intrinsic dynamical planes (IDPs)* and whose observed manifestation is the Fundamental Plane.

To better view the IDP's, their relation to the VP and any possible evolution we plot them in Figure 1 for $z = 6$ (green), $z = 5$ (red), and $z = 4$ (blue). Points are the actual data for all the massive objects, shown in a projection where the $z = 4$ data are edge-on.

⁶We stress that all our objects here are velocity dispersion supported

Ellipses stand for the corresponding projections of the 1-sigma 3D ellipsoids (full lines) or 3-sigma (blue dashed line). The centers of the ellipses are the corresponding projections of the ellipsoid centers. Straight lines have the same directions as the major axes of the ellipses resulting from projections of the VPs ellipsoids. Two important results arise from this plot and Table 1. First, high- z massive galaxies are on IDP's which are clearly tilted relative to the VP. Second, we observe a mild evolution of the IDP between $z = 6$ and $z = 4$, primarily driven by changes in the average values \tilde{E}_{star} , \tilde{r}_{star} , \tilde{v}_{star} and not the plane parameters α_{star}^{3D} and γ_{star}^{3D} .

3. Discussion & Conclusions

To shed more light onto the tilt of the IDP with respect to the VP, and following the discussion in §1, we have first checked if there is a mass homology breaking, that is, if the parameter c_M^{vir} depends on M_{bo}^{star} . We have calculated its trend with stellar mass ($\log M_{bo}^{star} \propto \beta_{vir}^M \log c_M^{vir}$) and listed the best fit β_{vir}^M in Table 2. Within the error bars the correlation is consistent with zero. This means that stars accomodate the product of their spatial and velocity dispersion distributions (i.e., $r_{e,bo}^{star} \sigma_{bo}^{star}$) according to M_{vir} . Second, we have checked whether the mass ratio M_{bo}^{star}/M_{vir} correlates with M_{bo}^{star} . And in fact, we find that this ratio decreases for increasing stellar mass at any given z (cf. Table 2). Therefore, we expect the IDP to be tilted against the VP (as discussed in the Introduction and explained in Oñorbe et al. 2005, 2006). We further compared our results against a simulation with different star formation parameters and found no difference concerning the IDP tilt.

But how can we understand these trends with respect to scenarios of galaxy formation? In order to answer this question we need to additionally consider the ratio of hot and cold baryon mass inside r_{vir} (i.e. M_h^{hb}/M_h^{cb}) as a function of the mass scale. First we note that mass assembly of the objects we analyze is dominated by cold accretion mode, in consistency with Kereš et al. (2009) results with the entropy-conserving GADGET-2 code. Now, the best-fit parameters to the scaling relation $\log M_{bo}^{star} \propto \beta \log M_h^{hb}/M_h^{cb}$ are given in Table 2 again. There we find that the fraction of hot over cold baryons increases very significantly as we go to higher masses. We can further acknowledge from Table 2 that the overall baryon fraction $f_B \equiv M_h^{bar}/M_{vir}$ does not depend on M_{bo}^{star} . Both these results taken together imply that massive haloes have proportionally less cold gas available to be accreted from the halo and transformed into stars than less massive ones. This explains the trend of M_{bo}^{star}/M_{vir} with the mass scale found above. Further, it is worth noting that all the β slopes in Table 2 change from one z to another only within their errors.

Now, why is more hot gas relative to cold gas enclosed within the virial radius as M_{vir}

increases? To answer to this question we have to recall how massive galaxies assemble their mass. Very briefly, our simulations show that massive galaxies form from gaseous mass elements enclosed by overdense subvolumes within the simulation box. As predicted by the Adhesion Model (Gurbatov et al. 1989; Vergassola et al. 1994) we have found that gas is bi-phasic. Indeed, at a given time a distinction can be made between singular gaseous mass elements (as those that have already been involved in caustic, i.e., singularity, formation at this time) and regular ones (those that have not yet been trapped into a caustic and tend to be of low density). We have also found that, from a global point of view, mass elements are dynamically organized as a hierarchy of *flow convergence regions* (FCRs), that is, attraction basins for mass flows. At high z FCRs undergo fast contractive deformations, that violently shrink them, transforming most of the cold, densest gaseous mass elements they contain into stars and heating the diffuse component there. Due to its low density, this component, once heated tends to keep hot along evolution, and forms shock fronts that expand, in consistency with Birnboim & Dekel (2003) results. We refer the reader to Domínguez-Tenreiro et al. (2010) for a more elaborate discussion.

In the simulations analyzed in this Letter, we have witnessed events occurring along the fast phase of massive galaxy formation, see §1: very fast mass assembly, dissipation and star formation rates ensuing FCR contractive deformations. These contractions act on dynamical timescales that are short because we have high overdensities where massive galaxies are about to form, therefore explaining the presence of massive objects in a young Universe. Additionally, such violent FCR contractions tend to swallow the mass close to them, severely limiting the amount of mass available to be further assembled after they occur. This would explain why a fraction of the objects we have identified are not dynamically disturbed. We have also seen in the simulations the gravitational gas heating due to these violent dynamical events, that partially transform the ordered mechanical energy involved in contractions into thermal energy and pressure. This is a crucial point for understanding the tilt of the IDP’s at high z ’s. To be quantitative, recall for example that a system must get rid of an amount of energy equal to its binding energy as it collapses from infinity and virializes (Binney & Tremaine 2008). This binding energy per unit virial mass increases with halo mass as $M_{\text{vir}}^{2/3}$, so that at assembling a galaxy, the more massive it is the more energy per unit mass is available to heat and pressurize the gas at the corresponding FCR contraction. Otherwise, as explained above, after these violent events most of the heated low density gas elements remain hot. This implies that more hot gas relative to cold gas is enclosed within r_{vir} as M_{vir} increases, as we have found. Therefore, we can conclude that the origin of the IDPs tilt relative to VPs lies in that gravitational gas heating processes are more effective as the mass of the halo increases and that there is not mass homology breaking. Finally, let us stress that the same physical processes act along the fast phase, as the slopes in Table 2

do not change with z s.

Summing up, the processes involved in high- z massive galaxy formation are: FCR contractions (approximatively equivalent to collapse) acting on a bi-phasic gas, induced by singularity formation in terms of the Adhesion Model approximation; the ensuing transformation of the ordered mechanical energy of contraction into velocity dispersion, and then partially into thermal energy and gas pressure, on the same timescales; and dense gas elements shrinkage, cooling and their transformation into stars. Energy injection is unlikely to substantially change the processes responsible for this high z FP tilt, because, as explained, they have to do with caustic (i.e. singularity) formation. We conclude that the violent processes described above are responsible for having: 1) massive objects at high redshift, 2) hot gas coronae, 3) less cold gas to form stars as the mass scale increases, because we have more gas heated, implying IDP's tilted relative to VP's, among other results. We see that the same processes are responsible for obtaining massive stellar objects shortly after the Big Bang as well as having them lying on IDPs: fast FCR contractions at different scales are the engine driving them.

We thank the anonymous referee for useful suggestions that improved the manuscript. We thankfully acknowledge to D. Vicente and J. Naranjo for the assistance and technical expertise provided at the Barcelona Supercomputing Centre, as well as the computer resources provided by BSC/RES (Spain). We thank DEISA Extreme Computing Initiative (DECI) for the CPU time allowed to GALFOBS project. The Centro de Computación Científica (UAM, Spain) has also provided computing facilities. This work was partially supported by the DGES (Spain) through the grants AYA2009-12792-C03-02/-03, as well as by the ASTROMADRID network (CAM S2009/ESP-1496). AK and JO were supported by the MICINN, Spain, through the Ramon y Cajal programme and the "Supercomputación y e-Ciencia" Consolider-Ingenio 2010 project (CSD2007-0050), respectively.

REFERENCES

- Bailin, J., et al. 2005, *ApJ*, 627, L17
- Binney J. & Tremaine S. 2008, *Galactic Dynamics*, Princeton University Press (Princeton, New Jersey)
- Birnboim, Y., & Dekel, A. 2003, *MNRAS*, 345, 349
- Bouwens, R. J., Illingworth, G. D., Franx, M., & Ford, H. 2007, *ApJ*, 670, 928

- Bouwens, R. J., et al. 2011, *Nature*, 469, 504
- Bryan, G.L. & Norman, M.L. 1998, *ApJ*, 495, 80
- Capak, P. L., et al. 2011, arXiv:1101.3586
- Cook M., Lapi A., Granato G. L., 2009, *MNRAS*, 397, 534
- Dahlen, T., et al. 2010, *ApJ*, 724, 425
- Domínguez-Tenreiro R., Oñorbe J., Sáiz A., Artal H., & Serna A. 2006, *ApJ*, 636, L77
- Domínguez-Tenreiro R., Oñorbe J., Martínez-Serrano F. J. & Serna A. 2010 *MNRAS*, accepted
- Dunkley, J., et al. 2009, *ApJS*, 180, 306
- Eggen O. J., Lynden-Bell D., Sandage A. R., 1962, *ApJ*, 136, 748
& Davé R. 2001, *ApJ*, 562, 605
- Giavalisco M., Dickinson M., Ferguson H. C., et al. 2004, *ApJ*, 600, L103
- Gurbatov S. N., Saichev A. I., Shandarin S. F., 1989, *MNRAS*, 236, 385
- Kereš, D., Katz, N., Fardal, M., Davé, R., & Weinberg, D. H. 2009, *MNRAS*, 395, 160
- Knollmann, S. R., & Knebe, A. 2009, *ApJS*, 182, 608
- Larson R. B., 1974, *MNRAS*, 166, 585
- Mancini, C., Matute, I., Cimatti, A., Daddi, E., Dickinson, M., Rodighiero, G., Bolzonella, M., & Pozzetti, L. 2009, *A&A*, 500, 705
- Martínez-Serrano, F. J., Serna, A., Domínguez-Tenreiro, R., & Mollá, M. 2008, *MNRAS*, 388, 3
- McLure, R. J., Cirasuolo, M., Dunlop, J. S., et al. 2006, *MNRAS*, 372, 357
- Mobasher B. et al., 2005, *ApJ*, 635, 832
- Mobasher B., Wiklind T., 2010, in *The Impact of HST on European Astronomy, Astrophysics and Space Science Proceedings*, F. Duccio Macchetto ed., Springer, Netherlands
- Oñorbe, J., Domínguez-Tenreiro R., Sáiz, A., Serna, A., Artal, H. 2005, *ApJ*, 632, L57
- Oñorbe, J., Domínguez-Tenreiro, R., Sáiz, A., Artal, H., Serna, A. 2006, *MNRAS*, 373, 503

- Oser, L., Ostriker, J. P., Naab, T., Johansson, P. H., & Burkert, A. 2010, arXiv:1010.1381
- Padmanabhan, T. 1993, *Structure Formation in the Universe*, by T. Padmanabhan, pp. 499. ISBN 0521424860. Cambridge, UK: Cambridge University Press, June 1993.
- Rodighiero, G., Cimatti, A., Franceschini, A., Brusa, M., Fritz, J., & Bolzonella, M. 2007, *A&A*, 470, 21
- Sáiz, A., Domínguez-Tenreiro, R., & Serna, A. 2004, *ApJ*, 601L, 131
- Salvador-Solé E., Manrique A., Solanes J. M. 2005, *MNRAS*, 358, 901
- Serna, A., Domínguez-Tenreiro, R., & Sáiz, A. 2003, *ApJ*, 597, 878
- Stark, D.P., Ellis, R.S., Bunker, A., Bundy, K., Targett, T., Benson, A., Lacy., 2009, *ApJ*, 697, 149
- Toomre A., 1977, in *The Evolution of Galaxies and Stellar Populations*, eds. B. Tinsley & R. Larson (New Have, CN: Yale Univ. Press)
- Vergassola M., Dubrulle B., Frisch U., Noullez A., 1994, *A&A*, 289, 325
- Wechsler R.H., Bullock J.S., Primack J.R., Kravtsov A.V., Dekel A., 2002, *ApJ*, 568, 52
- Weinberg, D. H., Hernquist, L., & Katz, N. 1997, *ApJ*, 477, 8
- White, S. D. M., & Rees, M. J. 1978, *MNRAS*, 183, 341
- Wiklind, T., Dickinson, M., Ferguson, H. C., et al. 2008, *ApJ*, 676, 781
- Yan, H., Dickinson, M., Giavalisco, M., et al. 2006, *ApJ*, 651, 24
- Zhao D.H., Mo H.J., Jing Y.P., Borner G., 2003, *MNRAS*, 339, 12

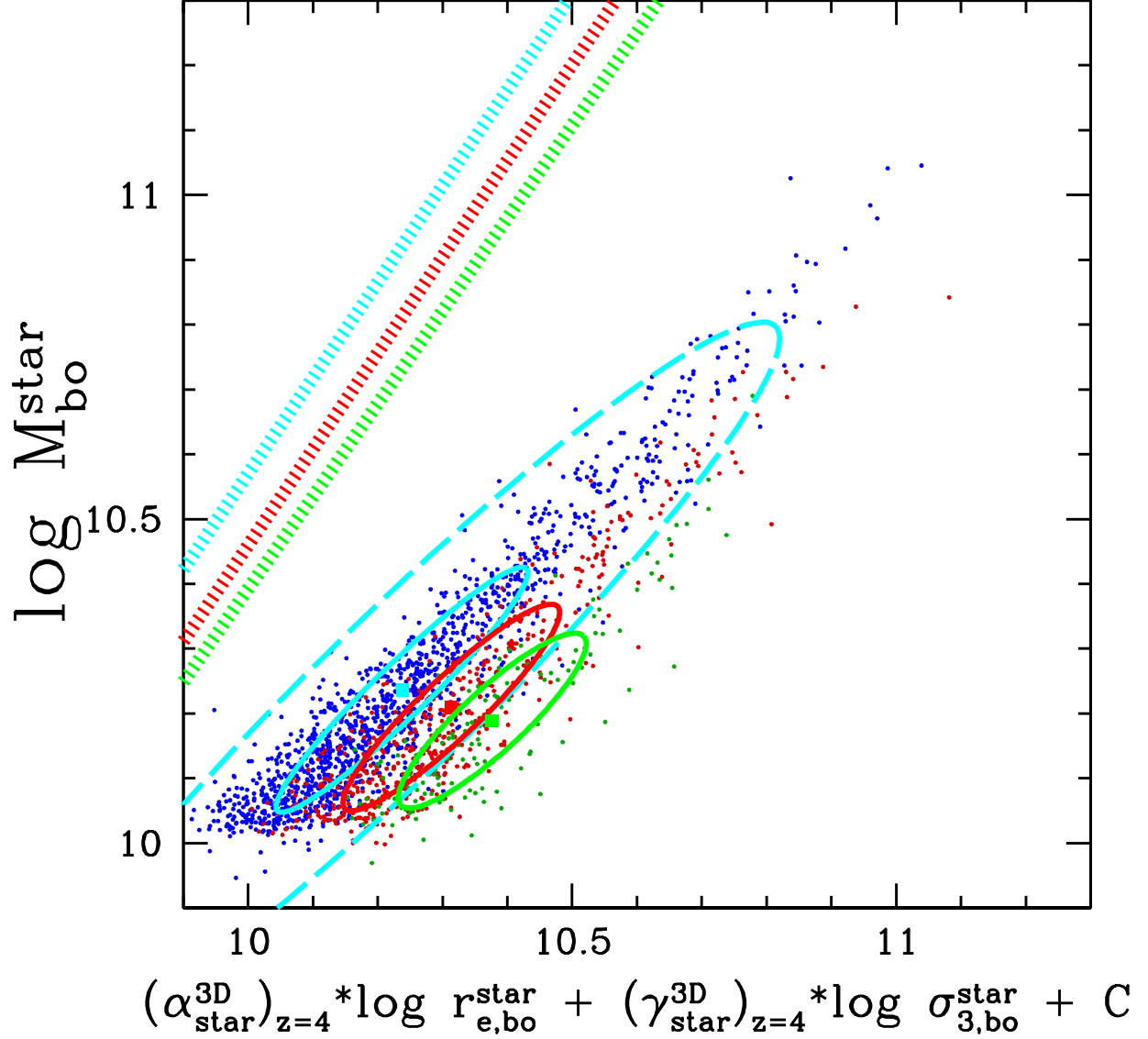


Fig. 1.— The $z = 4$ (blue), $z = 5$ (red) and $z = 6$ (green) IDPs seen in a projection where the $z = 4$ data are edge-on. Full line ellipses represent the corresponding $1 \times \sigma$ ellipsoids seen in the same projection. The $3 \times \sigma$ ellipse is also plotted for the $z = 4$ sample (long dashed line). The centers of the ellipses are the corresponding projections of the ellipsoid centers. Data points for all the massive objects in the samples are also plotted as circles using darker versions of their respective colours. Short dashed lines are the projections of the major axes of the VPs ellipsoids. $M_{\text{bo}}^{\text{star}}$ in M_{\odot} , $r_{\text{e,bo}}^{\text{star}}$ in kpc and $\sigma_{\text{bo}}^{\text{star}}$ in $km \times s^{-1}$.

Table 1. Results of PCA analysis.

Sample	No.	\tilde{E}	\tilde{r}	\tilde{v}	α^{3D}	γ^{3D}	σ_{Erv}
Halo							
$z = 6$	137	11.321 \pm 0.016	1.053 \pm 0.007	2.319 \pm 0.006	0.930 \pm 0.040	1.906 \pm 0.050	0.0100 \pm 0.0005
$z = 5$	521	11.326 \pm 0.010	1.118 \pm 0.005	2.284 \pm 0.003	0.822 \pm 0.017	2.008 \pm 0.024	0.0092 \pm 0.0003
$z = 4$	1315	11.336 \pm 0.007	1.188 \pm 0.003	2.248 \pm 0.003	0.798 \pm 0.013	2.053 \pm 0.018	0.0105 \pm 0.0002
Stellar							
$z = 6$	137	10.189 \pm 0.012	0.067 \pm 0.007	2.220 \pm 0.006	-0.142 \pm 0.091	2.096 \pm 0.104	0.0297 \pm 0.0021
$z = 5$	521	10.209 \pm 0.007	0.119 \pm 0.004	2.187 \pm 0.004	-0.002 \pm 0.059	2.040 \pm 0.052	0.0290 \pm 0.0010
$z = 4$	1315	10.237 \pm 0.005	0.189 \pm 0.003	2.146 \pm 0.003	0.077 \pm 0.035	1.994 \pm 0.027	0.0257 \pm 0.0006

Note. — Column 2: Number of massive galaxies in the sample. Columns 3, 4 and 5: sample mean values of the E , r and v variables ($\log M_{\odot}$, $\log kpc$ and $\log km \times s^{-1}$ respectively). Columns 6 and 7: coefficients of the IDP plane. Column 8: IDP orthogonal scatter in the E, r and v variables. Errors have been obtained from a bootstrapping analysis of the samples.

Table 2. Direct Fits.

X	β			ϕ		
	$z = 4$	$z = 5$	$z = 6$	$z = 4$	$z = 5$	$z = 6$
c_F	-0.071 \pm 0.009	-0.076 \pm 0.014	-0.045 \pm 0.033	1.0173	1.0500	0.7267
c_M^{vir}	0.059 \pm 0.032	0.019 \pm 0.066	0.074 \pm 0.142	0.8883	1.2765	0.6917
$(\sigma_h^{\text{tot}}/\sigma_{\text{bo}}^{\text{star}})^2$	-0.121 \pm 0.023	-0.131 \pm 0.046	-0.137 \pm 0.096	1.4470	1.5277	1.5876
$r_{e,h}^{\text{tot}}/r_{e,bo}^{\text{star}}$	0.252 \pm 0.025	0.225 \pm 0.046	0.256 \pm 0.110	-1.5761	-1.3013	-1.6227
$M_{\text{bo}}^{\text{star}}/M_{\text{vir}}$	-0.306 \pm 0.029	-0.258 \pm 0.057	-0.222 \pm 0.116	-2.0301	-1.5159	-1.1264
$M_h^{\text{hb}}/M_h^{\text{cb}}$	0.789 \pm 0.022	0.829 \pm 0.040	0.877 \pm 0.091	-8.8637	-9.2277	-9.6826
$M_h^{\text{bar}}/M_{\text{vir}}$	-0.061 \pm 0.006	-0.048 \pm 0.009	-0.032 \pm 0.142	-0.1594	-0.2892	-0.4581

Note. — Correlation between various properties X and $M_{\text{bo}}^{\text{star}}$ as derived from fitting $\log M_{\text{bo}}^{\text{star}} = \beta \log X + \phi$. Errors stand for a 97.5% confidence level intervals.